PNAS RESEARCH ARTICLE | BIOPHYSICS AND COMPUTATIONAL BIOLOGY

A diminished hydrophobic effect inside the GroEL/ES cavity contributes to protein substrate destabilization

Ilia Korobko[a,1], Robin Benjamin Eberle[a,1], Mousam Roy[a], and Amnon Horovitz[a,2]

Edited by Lila Gierasch, University of Massachusetts Amherst, Amherst, MA; received August 1, 2022; accepted October 20, 2022

Confining compartments are ubiquitous in biology, but there have been few experimental studies on the thermodynamics of protein folding in such environments. Recently, we reported that the stability of a model protein substrate in the GroEL/ES chaperonin cage is reduced dramatically by more than 5 kcal mol^{-1} compared to that in bulk solution, but the origin of this effect remained unclear. Here, we show that this destabilization is caused, at least in part, by a diminished hydrophobic effect in the GroEL/ES cavity. This reduced hydrophobic effect is probably caused by water ordering due to the small number of hydration shells between the cavity and protein substrate surfaces. Hence, encapsulated protein substrates can undergo a process similar to cold denaturation in which unfolding is promoted by ordered water molecules. Our findings are likely to be relevant to encapsulated substrates in chaperonin systems, in general, and are consistent with the iterative annealing mechanism of action proposed for GroEL/ES.

chaperonins | protein folding | hydrophobic effect | confinement

Significance

Protein confinement in compartments is ubiquitous in biology. Here, we show that a protein encapsulated in the GroEL/ES chaperonin cage is strongly destabilized owing, at least in part, to a diminished hydrophobic effect. Hence, encapsulated protein substrates can undergo a process similar to cold denaturation in which the relatively ordered water in the cavity contributes to unfolding. Our results suggest that cavity-confined water can lead to protein unfolding in other biological compartments such as the proteasome.

Chaperonins are large biomolecular machines that assist protein folding in vivo and in vitro in an ATP-dependent manner (for recent reviews see refs. 1–4). The GroE chaperonin system from *Escherichia coli* has become a paradigm for biomolecular machines, in general, and chaperonins in particular. It comprises GroEL, which is formed by two back-to-back stacked homo-heptameric rings, and its co-factor GroES, which is a homo-heptameric single-ring. GroES can bind to either one or both ends of GroEL in an ATP-dependent fashion, thereby forming 1:1 GroEL–GroES bullet-shaped (5) or 1:2 GroEL–$GroES_2$ football-shaped (6, 7) complexes, respectively. Binding of GroES to GroEL generates a cavity (also called "Anfinsen cage") in which substrate proteins become encapsulated and, thus, protected from aggregation. Despite more than three decades of intensive research, it remains unclear whether GroEL's function is limited to prevention of aggregation (8) and the folding process itself is not affected by GroEL (9) or if it has an "active" mechanism. Two ostensibly opposite kinetic effects have been attributed to GroEL in support of its active mechanism: acceleration of folding (3, 10–12) and unfolding (or "unfoldase") activity (4, 13–15). One reason for these seemingly conflicting findings may be that a universal mechanism of GroEL action does not exist, i.e., its mechanism may be substrate dependent. A second reason is that GroEL cycles between various states with different effects on substrate folding that have been difficult to disentangle. The apo state of GroEL, for example, has a higher affinity for nonfolded over folded states of substrate proteins since its cavity walls are hydrophobic (5). Consequently, the conformational equilibrium of substrates, in the presence of apo GroEL, is shifted in favor of their non-folded states (14, 16, 17). Adenosine 5'-triphosphate (ATP) and GroES binding-promoted conformational changes (13), which follow substrate binding, can cause bound misfolded proteins to undergo forced unfolding due to a stretching force applied to them. Such forced unfolding can lead to enhanced folding rates and yields according to the iterative annealing model (4). Finally, encapsulation in the GroEL/ES cavity can also affect the protein substrate's energy landscape.

Factors that can influence the folding properties of a protein substrate in the cavity include confinement, the chemical properties of the cavity walls and cavity-confined water, and the presence of GroEL's C-terminal tails. Simulations showed that confinement can either enhance or retard folding rates depending on the temperature and the interaction of the substrate with the cavity walls (18, 19). In another simulation study, it was proposed that folding in the GroES-capped cavity might be enhanced owing to the accumulation of water molecules near polar residues that line the cavity surface (20). This proposal is in accord with experimental work that indicated that removal of negatively charged residues in the cavity walls can retard folding (21). Stimulation of protein folding in the GroEL cavity has also been attributed to the presence of GroEL's C-terminal tails, which contain multiple Gly-Gly-Met motifs (22). The expected stabilizing effect of confinement and the observed acceleration of protein folding in the GroEL cavity suggested that encapsulated proteins are stabilized. In contrast, it was shown recently (23) that the stability

Author affiliations: [a]Department of Chemical and Structural Biology, Weizmann Institute of Science, Rehovot 7610001, Israel

Author contributions: A.H. designed research; I.K., R.B.E., and M.R. performed research; I.K., R.B.E., M.R., and A.H. analyzed data; and A.H. wrote the paper.

The authors declare no competing interest.

This article is a PNAS Direct Submission.

[1]I.K. and R.B.E. contributed equally to this work.

[2]To whom correspondence may be addressed. Email: Amnon.Horovitz@weizmann.ac.il.

This article contains supporting information online at https://www.pnas.org/lookup/suppl/doi:10.1073/pnas.2213170119/-/DCSupplemental.

Published November 21, 2022.

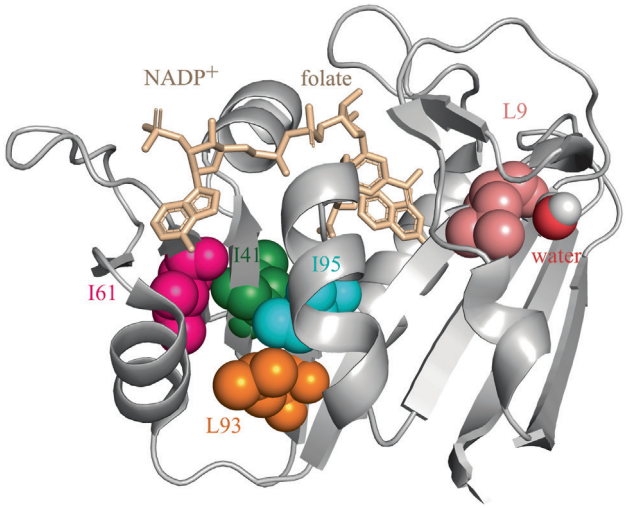

Fig. 1. Ribbon diagram of the crystal structure of dihydrofolate reductase from *Moritella profunda* (PDB ID: 2zza). The residues targeted for mutagenesis are shown using a space-filling representation and indicated using the single-letter code for amino acids. Also shown are the bound ligands, NADP+ and folate (in wheat color), and a water molecule bound to L9. The figure was generated using PyMOL.

of an encapsulated model substrate (that cannot escape into bulk solution) is reduced by more than 5 kcal mol^{-1} in comparison with its stability in bulk solution. Fluorescence anisotropy decay measurements showed free mobility of the encapsulated substrate, thereby indicating that its destabilization is unlikely to be due to interactions with the cavity walls (23). Here, we show that the destabilization of this substrate is due, at least in part, to a diminished hydrophobic effect in the cavity.

Results and Discussion

Experimental Approach. The magnitude of the hydrophobic contribution to protein stability inside the GroEL cavity was probed by truncating buried aliphatic side chains in dihydrofolate reductase from *Moritella profunda* ($DHFR_{Mp}$) fused to the C terminus of enhanced green fluorescent protein (eGFP) (23). $DHFR_{Mp}$ is a useful model substrate since it is relatively unstable at room temperature (23, 24) and its folding can be monitored easily by measuring the regain in enzyme activity. $DHFR_{Mp}$ was fused to eGFP in order to further destabilize it (25, 26) and to facilitate determination of its location, i.e., whether it is in the cavity or has escaped. Five buried aliphatic residues in $DHFR_{Mp}$ (Fig. 1 and Table 1), which are distant from its NADPH and dihydrofolate binding sites, were targeted for mutagenesis. Their side chains were truncated via Ile→Val or Leu→Val mutations, thereby removing a methylene group. Such truncations have been widely employed to assess the hydrophobic contribution to protein stability (27, 28). Under ideal circumstances, these truncations result in loss of the free energy of transfer of a methylene group from water to the protein's hydrophobic interior and a change in free energy due to local packing alterations, but global rearrangements and stability effects due to changes in side-chain and main-chain entropies are minimal.

Effects of Hydrophobic Core Mutations on Stability in Bulk Solution. The effects of the mutations in $DHFR_{Mp}$ fused to eGFP on its stability in bulk solution were measured by guanidinium hydrochloride denaturation as described (23). These measurements were carried out in the presence of different concentrations of NADPH in order to minimize aggregation that takes place in bulk solution. The free energy of folding in the absence of NADPH was then obtained via linear extrapolation (Fig. 2 and Dataset S1). It may be seen (Table 1) that all the mutations are destabilizing in bulk solution as expected when a buried methylene group is removed. The effects of some of the mutations are perhaps smaller than expected because the cores of psychrophilic proteins are less well packed and the contribution of the hydrophobic effect to their stability is less dominant than in the case of mesophilic proteins (29, 30). Nevertheless, the average mutational effect we observe of 0.8 kcal mol^{-1} with a SD of 0.7 kcal mol^{-1} is in close agreement with the value of 0.9 kcal mol^{-1} with a SD of 0.8 kcal mol^{-1} reported before for a large dataset of hydrophobic core replacements (28).

Effects of Hydrophobic Core Mutations on Protein Stability in the GroEL/ES Cavity. Previous work showed that eGFP encapsulated in football-shaped GroEL-$GroES_2$ complexes, in the presence of BeF_x, does not escape into bulk solution even after overnight incubation at room temperature (23). Such stable encapsulation is also found for $DHFR_{Mp}$ fused to eGFP (*SI Appendix*, Fig. S1). The effects of mutations in $DHFR_{Mp}$ fused to eGFP on its stability in the GroEL cavity were determined by following the change in

Table 1. Stabilities of $DHFR_{Mp}$ variants fused to eGFP in bulk solution and in the GroE and thermosome cavities

Protein*	Exposed surface area of mutated residue in the native state (Å^2)†	Percent area of mutated residue exposed in the native state†	Stability in bulk solution (kcal mol^{-1})	Change in stability in bulk solution upon mutation (kcal mol^{-1})‡	Stability in the cavity (kcal mol^{-1})	Change in stability in the cavity upon mutation (kcal mol^{-1})‡
WT in GroE§	-	-	−3.45 ± 0.09	-	2.4 ± 0.2	-
WT in $(\alpha\beta)_4$	-	-	−3.45 ± 0.09	-	2.7 ± 0.3	-
WT in β_9	-	-	−3.45 ± 0.09	-	3.3 ± 0.2	-
L9V in GroE	4.0	3.5	−2.60 ± 0.13	0.85 ± 0.15	3.7 ± 0.3	1.3 ± 0.4
I41V in GroE	0.0	0	−2.95 ± 0.07	0.50 ± 0.11	1.6 ± 0.1	−0.8 ± 0.2
I61V in GroE	0.1	0	−3.16 ± 0.07	0.29 ± 0.11	2.2 ± 0.2	−0.2 ± 0.3
L93V in GroE	5.4	4.0	−1.52 ± 0.18	1.93 ± 0.20	0.9 ± 0.1	−1.5 ± 0.2
I95V in GroE	5.8	3.5	−3.03 ± 0.09	0.42 ± 0.13	2.8 ± 0.3	0.4 ± 0.4

*Single-letter notation of amino acids is used.
†Values represent averages for the two dihydrofolate reductase chains (A and B) related by noncrystallographic symmetry in the crystal structure (PDB ID: 2zza). The solvent-accessible surface areas for each residue listed were calculated using PyMOL.
‡The changes in stability in bulk solution and in the cavity upon mutation were calculated as: ΔG(mutant) – ΔG(wild-type).
§The data for wild-type $DHFR_{Mp}$ in the chimera were reported before (23).

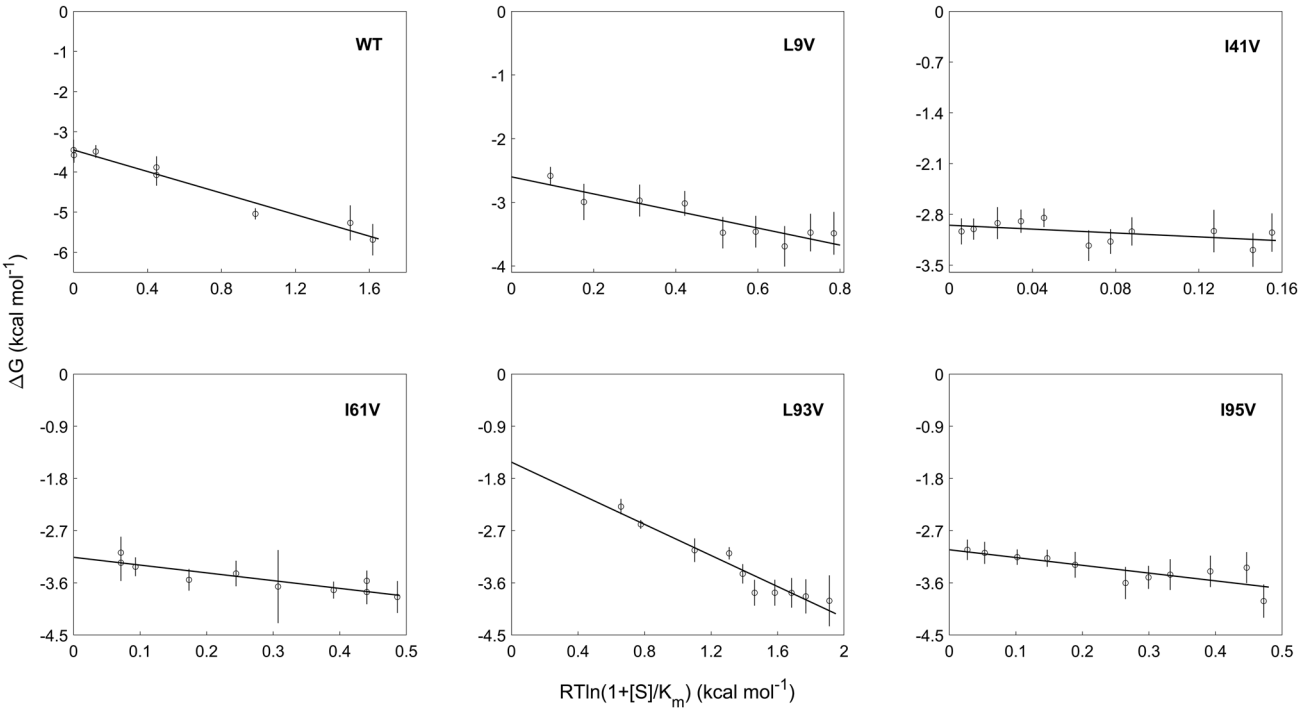

Fig. 2. Stability measurements of the $DHFR_{Mp}$ part of the chimera in bulk solution. The stability of the $DHFR_{Mp}$ part of the chimera was determined as a function of GuHCl concentration at different fixed concentrations of NADPH. Shown are the free energies of unfolding, in the absence of GuHCl, plotted against a function of the concentration of NADPH (S) for wild-type $DHFR_{Mp}$ and the L9V, I41V, I61V, L93V, and I95V mutants. The data were fitted using Eq. **2**. The y-intercepts correspond to the free energies of folding in bulk solution provided in Table 1. Error bars represent SE.

absorbance at 340 nm, upon addition of the substrate dihydrofolate (DHF) and NADPH, as before (23). The enzymatic activity of encapsulated $DHFR_{Mp}$ in the chimera displays a lag phase, which is absent when the chimera is free in bulk solution (23). The value of the rate constant associated with the lag phase decreases with increasing substrate (DHF) concentrations (Fig. 3). Such a decrease is diagnostic for a conformational selection mechanism, i.e., when there is an equilibrium between the unfolded and folded forms of $DHFR_{Mp}$ in the chimera that is shifted in favor of the folded form in the presence of DHF. The decrease occurs because the rate of approach to equilibrium shifts from the reversible interconversion between the folded and unfolded states at low DHF concentrations (described by the sum of folding (k_f) and unfolding (k_u) rate constants) to an irreversible switch to the folded form at high DHF concentrations described by k_f only. Consequently, estimates of k_f and k_u can be extracted from plots of the observed rate constant as a function of DHF concentration (see Eq. **4** in *Methods*) from which the free energy of folding can be calculated. Previous work showed that wild-type $DHFR_{Mp}$ in the chimera is destabilized by more than 5 kcal mol^{-1} in the GroEL/ES cavity relative to bulk solution (23). A similar destabilization by more than 5 kcal mol^{-1} is also observed when $DHFR_{Mp}$ fused to eGFP is encapsulated in the cavity of the thermosome from *Sulfolobus acidocaldarius*, an archaeal homolog of GroEL, formed by α and β subunits ($(\alpha\beta)_4$ rings) or only β subunits (β_9 rings) (Fig. 3), thereby indicating that it may apply to chaperonins, in general, and, perhaps, to other confining systems.

Strikingly, although the truncations of buried aliphatic side chains in $DHFR_{Mp}$ are all found to be destabilizing within error in bulk solution, their effects in the GroEL/ES cavity are idiosyncratic but mostly neutral or even stabilizing (Table 1). The mutations I41V and L93V are stabilizing, whereas the mutations I61V and I95V have essentially no effect within error on stability. Three major effects associated with truncations of buried aliphatic side chains are i) destabilization due to loss of the free energy of transfer of a methylene group from water to the hydrophobic core; ii) changes in packing because of the void created in the protein interior; and iii) changes in side-chain entropies which can be stabilizing or destabilizing depending on the mutation and its location (28). Effects ii) and iii) are unlikely to differ much between bulk solution and the GroEL/ES cavity. Given that the loss of the free energy of transfer is always destabilizing, the neutral or stabilizing effects of the truncations observed here indicate that the hydrophobic effect in the GroEL/ES cavity is diminished. The effects of mutations in the cavity are, therefore, due to a balance between packing changes, which occur only if they are stabilizing, and changes in side-chain entropy which can be stabilizing or destabilizing. The effect of the L9V mutation differs and is destabilizing, but L9 has a bound water molecule in the native state (Fig. 1). Hence, L9 might be less buried in solution than in the crystal structure, and the destabilizing effect of this mutation is more likely to be due to factors other than loss of the free energy of transfer (such as changes in packing or side-chain entropy) that are similar in the cavity and bulk solution.

Why could the hydrophobic effect be diminished in the cavity? Given that $DHFR_{Mp}$ fused to the eGFP substrate is not bound to the cavity walls (23) and that the volumes of the cavity and the substrate are 175,000 $Å^3$ (5) and 58,000 $Å^3$ (23), respectively, it is easy to calculate that the average distance (over time and space) between the cavity walls and the substrate surface is about 10 Å (assuming that both the cavity and the substrate are spherical) (Fig. 4). Such a distance corresponds to about three hydration layers comprising two first shells and one second shell (31) which are relatively ordered, thereby resulting in a diminished hydrophobic effect. This is somewhat analogous to protein cold denaturation, which is believed to result from a weaker hydrophobic effect owing to water ordering at lower temperatures. It is important to note that the average distance between the cavity walls and

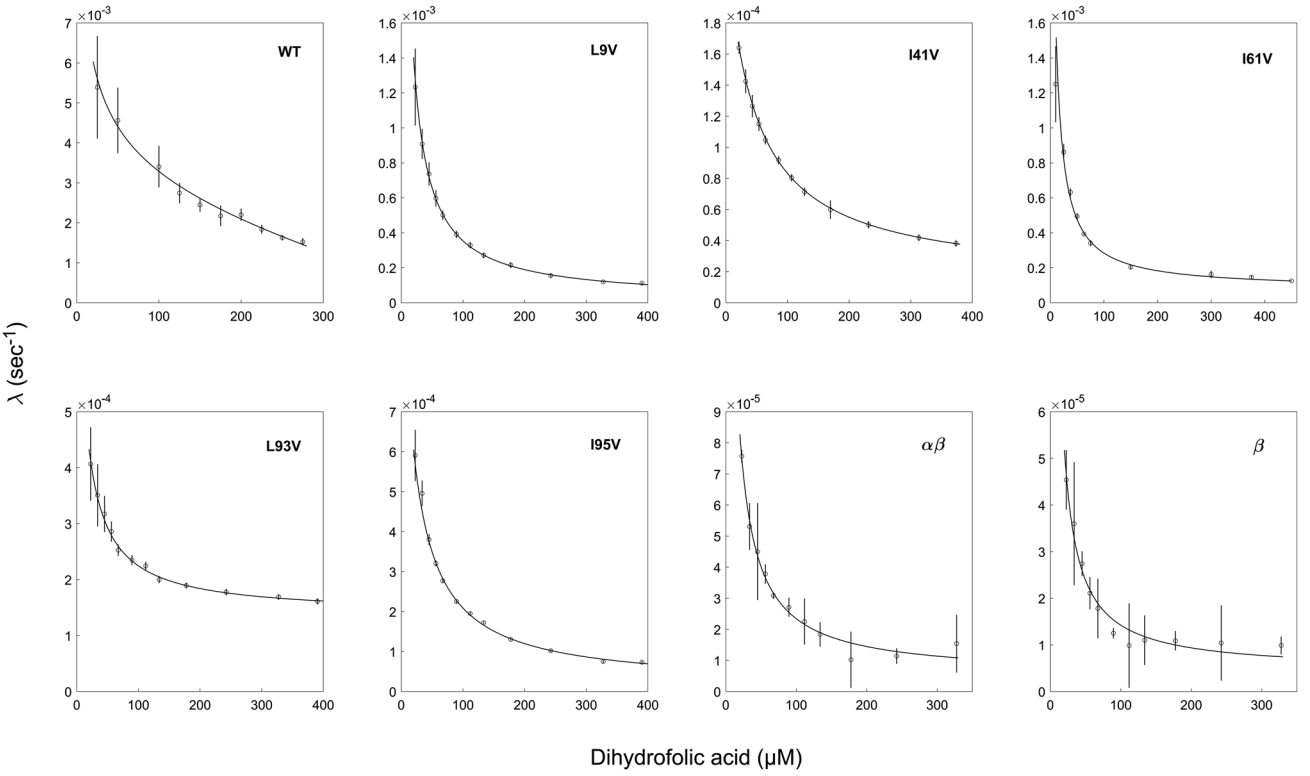

Fig. 3. Encapsulation in the GroE and thermosome cavities affects folding of the $DHFR_{Mp}$ part of the chimera. Representative plots of the observed rate constant, λ, as a function of dihydrofolic acid concentration are shown for the indicated mutants of the $DHFR_{Mp}$ part of the chimera inside the GroE cavity. Also shown are such plots for folding of the wild-type version of the $DHFR_{Mp}$ part of the chimera inside the cavities of the thermosome from *Sulfolobus acidocaldarius* formed by α and β subunits $((\alpha\beta)_4$ rings) or only β subunits (β_9 rings). The data were fitted to Eq. **4**, thereby yielding estimates of the folding and unfolding rate constants. The free energies of folding are provided in Table 1. All the experiments were carried out at least in duplicate. Error bars represent SE.

the surface of a 30-kDa substrate would be about 13 Å, which is equivalent to four hydration shells. Consequently, destabilization inside the GroEL/ES cavity owing to a diminished hydrophobic effect is expected from such calculations also for smaller protein substrates. In fact, there is evidence that some ordering of cavity -confined water molecules occurs even in the absence of an encapsulated substrate (32). Our analysis is also in agreement with simulations of smaller systems comprising nanotube-confined villin (33) or a 23-residue helical peptide (34), which showed that they become unstructured owing to reduced solvent entropy.

The destabilizing effect of encapsulation in the thermosome and GroEL/ES cavities is in agreement with the iterative annealing mechanism of action, according to which misfolded proteins are unfolded, thereby giving them further opportunity to fold correctly (4). It has been reported that protein substrates become unfolded in the cavity first upon binding to GroEL's apo state and then because of forced unfolding due to ATP and GroES binding-promoted conformational changes (13). Our results show that the unfolded state is reached also because it is strongly favored thermodynamically owing to a diminished hydrophobic effect in the GroES-capped cavity. It is important to note, however, that the unfolded state in the cavity is likely to differ from that in bulk solution because of confinement. In conclusion, the results reported here should also be relevant to other confining compartments such as the proteasome where unfolding promoted by a reduced hydrophobic effect would facilitate protein degradation.

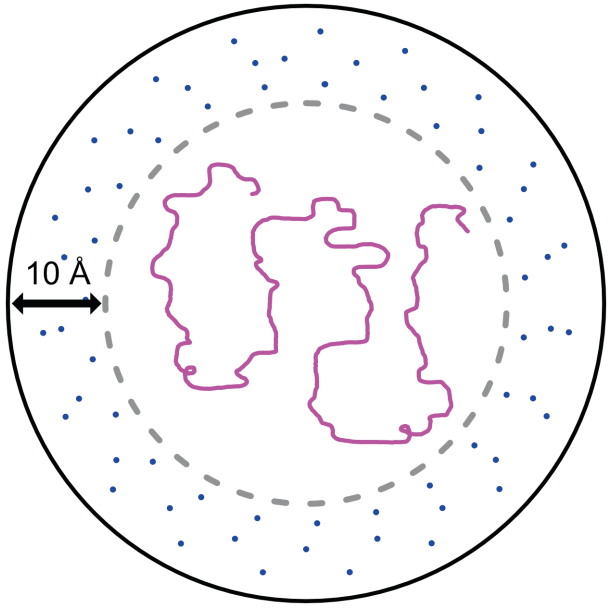

Fig. 4. Scheme showing encapsulated substrate in the GroEL/ES cavity. Assuming that both the cavity and the substrate are spherical with respective volumes of 175,000 $Å^3$ (5) and 58,000 $Å^3$ (23) and given that the $DHFR_{Mp}$ fused to eGFP substrate is not bound to the cavity walls (23), it is easy to calculate that the average distance between the cavity walls and substrate surface is about 10 Å. Such a distance corresponds to about three relatively ordered hydration shells, thereby resulting in a diminished hydrophobic effect.

Methods

Molecular Biology. Mutations in $DHFR_{Mp}$ fused to eGFP were introduced by amplifying the previously constructed gene for this chimera in a Pet21a plasmid (23) using restriction-free cloning. The L9V, I41V, I61V, L93V, and I95V mutants were constructed using the forward primer

5′-GTCTACTTGAAAGAGTCAAACTCGAGTGAACTCGAGCACCACCACCACC-3′ and the respective reverse primers: 5′-GATTGCCGCAGTAGCGAATA-3′;

5′-GGGTAAACCAGTCGTAATGGGCAG-3′; 5′-GCAGACTAAATGTAGTCCTGTCTAG-3′; 5′-CGTAGAAGAGGTAATGATCATTGG-3′; and 5′-GTAGAAGAGCTTATGGTAATTGGCG-3′. All the mutations were verified by DNA sequencing of the entire gene.

Protein Expression and Purification. The wild-type and mutant versions of the chimera of $DHFR_{Mp}$ fused to eGFP were expressed and purified as before (23). GroEL and GroES were expressed as described (35). The cells were then resuspended in 20 mM Tris-HCl buffer (pH 7.5) containing 60 mM KCl, 10 mM $MgCl_2$, 2 mM dithiothreitol (DTT), 0.1 mM ethylenediaminetetraacetic acid (EDTA), and 0.5 mM phenylmethylsulfonyl fluoride (PMSF) and disrupted using sonication. The cell lysate was centrifuged at 47,850 *g* for 30 min at 4°C, and the supernatant was then subjected to 55% ammonium sulfate precipitation. The pellet was then resuspended in buffer A (50 mM Tris-HCl (pH 7.5) containing 10 mM imidazole, 500 mM NaCl, and 10 mM β-mercaptoethanol) and loaded on a HisTrap 5-ml HP column (GE Healthcare) equilibrated with this buffer. The flow-through was collected, subjected to ammonium sulfate precipitation, and used for GroEL purification (see below). GroES was eluted using a linear gradient of 10–500 mM imidazole in buffer A. GroES-containing fractions were combined, warmed to 60°C for 15 min, and centrifuged at 38,760 *g* for 30 min at 4°C. The supernatant containing GroES was concentrated and loaded on a Superose 6 10/300 GL column (GE Healthcare) equilibrated with G10K buffer (50 mM Tris-HCl (pH 7.5) containing 10 mM KCl, 10 mM $MgCl_2$ and 1 mM DTT). The GroES-containing fractions were combined and concentrated, and aliquots of the protein were snap-frozen in liquid nitrogen and stored at −80°C. The GroEL-containing pellet was resuspended in buffer B (50 mM Tris-HCl (pH 7.5) containing 0.1 mM EDTA and 1 mM DTT) and loaded on a 30-ml Q Sepharose column preequilibrated with buffer B. GroEL was eluted using a linear gradient of 0–1 M NaCl in buffer B. GroEL-containing fractions were combined and subjected to ammonium sulfate precipitation as above. The pellet was then resuspended in buffer C (50 mM 2-(N-morpholino) ethanesulfonic acid (MES) (pH 6.0) containing 1 mM EDTA, 1 mM DTT, and 25% methanol) and loaded on a 1-ml MonoQ column (GE Healthcare) equilibrated with buffer C. GroEL was eluted using a 0–1 M NaCl gradient in buffer C. GroEL-containing fractions were pooled, subjected to 45% acetone precipitation for 10 min at room temperature, and then centrifuged at 30,600 *g* for 15 min at 4°C. The pellet was then dried, resuspended in G10K buffer, and loaded on a Superose 6 10/300 GL column (GE Healthcare) equilibrated with this buffer. The GroEL-containing fractions were combined and concentrated, and aliquots of the protein were snap-frozen in liquid nitrogen and stored at −80°C. Protein concentrations were determined as before (35).

Individual α and β subunits (with a C-terminal His-tag) of the thermosome from *Sulfolobus acidocaldarius* were expressed in Rosetta (DE3) cells harboring the pET Duet I and pET28a plasmids containing these respective genes. Cells were resuspended in lysis buffer (50 mM Tris-HCl (pH 8.0) 150 mM KCl, 10% glycerol, 1 mM lysozyme, and 1 mM PMSF) and lysed by sonication on ice (70% amplitude, 3 × 30-s pulse and 2-min interval between pulses). Cell debris was removed by centrifugation at 26,892 *g* for 30 min. The supernatant was further incubated at 60°C for 30 min followed by centrifugation at 26,892 *g* for 30 min. This step causes aggregation and separation of most of the *E. coli* proteins. The heat-treated lysate was then subjected to Ni-NTA affinity chromatography in 50 mM Tris-HCl (pH 8.0) buffer containing 150 mM KCl, 10% glycerol, and 10 mM imidazole, and elution was carried out using a gradient of 100–500 mM imidazole. Further purification of α and β subunits was achieved by size exclusion chromatography in 50 mM Tris-HCl (pH 8.0) buffer with 150 mM KCl on a Superdex 200 10/300 GL column. Formation of αβ heterooligomers was achieved by mixing the purified subunits in a 1:1 ratio in 50 mM Tris-HCl (pH 8.0) and 100 mM KCl followed by the addition of 25 mM $MgCl_2$ and 5 mM ATP. The mixture was then incubated at 75°C for 30 min. β homooligomers were obtained similarly using purified β subunits.

Stability Measurements of the $DHFR_{Mp}$ Part of the Chimera in Bulk Solution. The stabilities of mutants of the $DHFR_{Mp}$ part of the chimera were determined as a function of GuHCl concentration at different fixed concentrations of NADPH as before (23). The data were fitted to

$$F = \frac{F_U^0 + a[D] + \left(F_N^0 + b[D]\right) e^{\frac{-\Delta G^0 + m[D]}{RT}}}{1 + e^{\frac{-\Delta G^0 + m[D]}{RT}}}, \quad [1]$$

where ΔG^0 is the free energy of unfolding in the absence of denaturant, $[D]$ is the GuHCl concentration, m is the GuHCl-concentration dependence of the free energy of unfolding ($m = \frac{\partial \Delta G}{\partial [D]}$), T is the temperature, and R is the gas constant. The fluorescence of the native (F_N) and denatured (F_U) states are expressed as linear functions of the GuHCl concentration with slopes of a and b, respectively. This analysis is based on the assumption that the melting curves reflect the denaturation only of the $DHFR_{Mp}$ part of the chimera, which is justified since eGFP is very stable under our conditions and the fluorescence of its single tryptophan residue changes very little (and in a linear fashion) as a function of GuHCl concentration. The values of ΔG^0 obtained from the fits to Eq. **1** were then plotted as a function of the concentration of NADPH, and the data were fitted to

$$\Delta G = \Delta G^0 - RTln\left(1 + \frac{[S]}{K_m}\right), \quad [2]$$

where $[S]$ is the concentration of NADPH and K_m is the Michaelis–Menten constant whose value can be mutant dependent. Here, ΔG^0 is the free energy of unfolding in the absence of both GuHCl and NADPH. Eq. **2** is derived by assuming that the substrate, *S*, binds only to the folded state, *F*. Consequently, the apparent folding equilibrium constant, *K*, is given by: $K = \frac{[F]+[FS]}{[U]} = \frac{[F]+[F][S]/K_m}{[U]} = K^0\left(1 + \frac{[S]}{K_m}\right)$. Taking the logarithm of both sides of the latter equation and multiplying by $-RT$ yields Eq. **2**.

Activity Assays of Encapsulated $DHFR_{Mp}$. Encapsulation of wild-type and mutant versions of $DHFR_{Mp}$ fused to eGFP in the cavities of chaperonin footballs was achieved as described (23). The enzyme activity of the encapsulated $DHFR_{Mp}$ was monitored as before (23) by following the change in the absorbance at 340 nm, in the presence of different concentrations of DHF and a fixed concentration of NADPH. The data were fitted to

$$[P] = Vt + A(e^{-\lambda t} - 1), \quad [3]$$

where $[P]$ is the product concentration (or the absorbance at 340 nm which is proportional to it), V is the slope that corresponds to the linear steady-state velocity of the reaction, and A and λ are the respective amplitude and rate constant of the lag phase. Eq. **3** can be derived for the reaction scheme $E_U \rightleftarrows E_F \rightleftarrows ES$, where E_U, E_F, and ES designate the respective unfolded, folded, and substrate-bound folded states of $DHFR_{Mp}$ (E), assuming that ligand binding is fast relative to the folding and unfolding steps. In such a case of conformational selection, the rate constant, λ, is given by:

$$\lambda = k_f + \frac{k_u k_{-1}}{k_1[S] + k_{-1}} = k_f + \frac{k_u}{K_a[S] + 1}, \quad [4]$$

where k_f and k_u are the respective folding and unfolding rate constants, k_1 and k_{-1} are the respective substrate association and dissociation rate constants, and $K_a = k_1/k_{-1}$ is the substrate association constant. A detailed derivation of Eq. **4** has been provided before (23). In brief, the rates of changes in the concentrations of E_U, E_F, and ES, in the case of the above reaction scheme, are given by

$$d[E_U]/\mathrm{dt} = -k_f[E_U] + k_u[E_F]. \quad [5]$$

$$d[E_F]/\mathrm{dt} = k_f[E_U] - \left(k_u + k_1[S]\right)[E_F] + k_{-1}[\mathrm{ES}], \quad [6]$$

$$d[\mathrm{ES}]/\mathrm{dt} = k_1[S][E_F] - k_{-1}[\mathrm{ES}]. \quad [7]$$

These three rate equations can be expressed in a matrix form, as follows:

$$\begin{bmatrix} k_f - \lambda & -k_u & 0 \\ -k_f & k_u + k_1[S] - \lambda & -k_{-1} \\ 0 & -k_1[S] & k_{-1} - \lambda \end{bmatrix} \begin{bmatrix} [E_U] \\ [E_F] \\ [ES] \end{bmatrix} = 0, \quad [8]$$

where λ is the apparent rate constant. Given that the determinant of the above matrix must be equal to zero, there are two solutions for λ given by

$\lambda_1 + \lambda_2 = k_f + k_u + k_1[S] + k_{-1}$ and $\lambda_1\lambda_2 = k_f k_1 + k_f k_{-1} + k_u k_{-1}$. Eq. **4** is obtained by assuming that ligand binding is much faster than folding, i.e.,

$\lambda_2 = k_1[S] + k_{-1}$. Inspection of Eq. **4** shows that the value of the observed rate constant, λ, decreases with increasing substrate concentration as observed before (23) and here (Fig. 3). Estimates of the folding and unfolding rate constants were obtained from fits of λ vs. DHF concentration to Eq. **4**.

Data, Materials, and Software Availability. All study data are included in the article and/or *SI Appendix*. The underlying data for Figs. 2 and 3 are provided in Datasets S1 and S2, respectively.

ACKNOWLEDGMENTS. We thank Profs. Fred Naider and Keith Willison for critical reading of an earlier version of this paper, Dr. Harry Greenblatt for helpful advice, and Edo Kiper for help in constructing a mutant. This work was supported by grant 2021077 of the US-Israel Binational Science Foundation, an Israel Science Foundation grant (842/20), and the Kimmelman Center for Biomolecular Structure and Assembly. A.H. is an incumbent of the Carl and Dorothy Bennett Professorial Chair in Biochemistry.

1. A. Horovitz, T. H. Reingewertz, J. Cuéllar, J. M. Valpuesta, Chaperonin mechanisms: Multiple and (mis)understood? *Annu. Rev. Biophys.* **51**, 115–133 (2022).
2. A. L. Horwich, W. A. Fenton, Chaperonin-assisted protein folding: A chronologue. *Q. Rev. Biophys.* **53**, e4 (2020).
3. D. Balchin, M. Hayer-Hartl, F. U. Hartl, Recent advances in understanding catalysis of protein folding by molecular chaperones. *FEBS. Lett.* **594**, 2770–2781 (2020).
4. D. Thirumalai, G. H. Lorimer, C. Hyeon, Iterative annealing mechanism explains the functions of the GroEL and RNA chaperones. *Protein Sci.* **29**, 360–377 (2020).
5. Z. Xu, A. L. Horwich, P. B. Sigler, The crystal structure of the asymmetric GroEL-GroES-$(ADP)_7$ chaperonin complex. *Nature* **388**, 741–750 (1997).
6. A. Koike-Takeshita, T. Arakawa, H. Taguchi, T. Shimamura, Crystal structure of a symmetric football-shaped GroEL:$GroES_2$-ATP_{14} complex determined at 3.8 Å reveals rearrangement between two GroEL rings. *J. Mol. Biol.* **426**, 3634–3641 (2014).
7. X. Fei, X. Ye, N. A. LaRonde, G. H. Lorimer, Formation and structures of GroEL:$GroES_2$ chaperonin footballs, the protein-folding functional form. *Proc. Natl. Acad. Sci. U.S.A.* **111**, 12775–12780 (2014).
8. A. L. Horwich, A. C. Apetri, W. A. Fenton, The GroEL/GroES *cis* cavity as a passive anti-aggregation device. *FEBS Lett.* **583**, 2654–2662 (2009).
9. H. Hofmann *et al.*, Single-molecule spectroscopy of protein folding in a chaperonin cage. *Proc. Natl. Acad. Sci. U.S.A.* **107**, 11793–11798 (2010).
10. F. Georgescauld *et al.*, GroEL/ES chaperonin modulates the mechanism and accelerates the rate of TIM-barrel domain folding. *Cell* **157**, 922–934 (2014).
11. X. Ye, L. Mayne, Z. Y. Kan, S. W. Englander, Folding of maltose binding protein outside of and in GroEL. *Proc. Natl. Acad. Sci. U.S.A.* **115**, 519–524 (2018).
12. A. K. Singh, D. Balchin, R. Imamoglu, M. Hayer-Hartl, F. U. Hartl, Efficient catalysis of protein folding by GroEL/ES of the obligate chaperonin substrate MetF. *J. Mol. Biol.* **432**, 2304–2318 (2020).
13. Z. Lin, D. Madan, H. S. Rye, GroEL stimulates protein folding through forced unfolding. *Nat. Struct. Mol. Biol.* **15**, 303–311 (2008).
14. S. Priya *et al.*, GroEL and CCT are catalytic unfoldases mediating out-of-cage polypeptide refolding without ATP. *Proc. Natl. Acad. Sci. U.S.A.* **110**, 7199–7204 (2013).
15. E. Koculi, D. Thirumalai, Retardation of folding rates of substrate proteins in the nanocage of GroEL. *Biochemistry* **60**, 460–464 (2021).
16. R. Zahn, S. Perrett, G. Stenberg, A. R. Fersht, Catalysis of amide proton exchange by the molecular chaperones GroEL and SecB. *Science* **271**, 642–645 (1996).
17. D. S. Libich, V. Tugarinov, G. M. Clore, Intrinsic unfoldase/foldase activity of the chaperonin GroEL directly demonstrated using multinuclear relaxation-based NMR. *Proc. Natl. Acad. Sci. U.S.A.* **112**, 8817–8823 (2015).
18. M. R. Betancourt, D. Thirumalai, Exploring the kinetic requirements for enhancement of protein folding rates in the GroEL cavity. *J. Mol. Biol.* **287**, 627–644 (1999).
19. A. Baumketner, A. Jewett, J. E. Shea, Effects of confinement in chaperonin assisted protein folding: Rate enhancement by decreasing the roughness of the folding energy landscape. *J. Mol. Biol.* **332**, 701–713 (2003).
20. J. L. England, D. Lucent, V. S. Pande, A role for confined water in chaperonin function. *J. Am. Chem. Soc.* **130**, 11838–11839 (2008).
21. Y. C. Tang *et al.*, Structural features of the GroEL-GroES nano-cage required for rapid folding of encapsulated protein. *Cell* **125**, 903–914 (2006).
22. J. Weaver, H. S. Rye, The C-terminal tails of the bacterial chaperonin GroEL stimulate protein folding by directly altering the conformation of a substrate protein. *J. Biol. Chem.* **289**, 23219–23232 (2014).
23. I. Korobko, H. Mazal, G. Haran, A. Horovitz, Measuring protein stability in the GroEL chaperonin cage reveals massive destabilization. *eLife* **9**, e56511 (2020).
24. Y. Xu, G. Feller, C. Gerday, N. Glansdorff, *Moritella* cold-active dihydrofolate reductase: Are there natural limits to optimization of catalytic efficiency at low temperature? *J. Bacteriol.* **185**, 5519–5526 (2003).
25. M. Sokolovski, A. Bhattacherjee, N. Kessler, Y. Levy, A. Horovitz, Thermodynamic protein destabilization by GFP tagging: A case of interdomain allostery. *Biophys. J.* **109**, 1157–1162 (2015).
26. K. Dave, H. Gelman, C. T. Thu, D. Guin, M. Gruebele, The effect of fluorescent protein tags on phosphoglycerate kinase stability is nonadditive. *J. Phys. Chem. B* **120**, 2878–2885 (2016).
27. J. T. Kellis Jr., K. Nyberg, D. Sali, A. R. Fersht, Contribution of hydrophobic interactions to protein stability. *Nature* **333**, 784–786 (1988).
28. J. B. Holder *et al.*, Energetics of side chain packing in staphylococcal nuclease assessed by exchange of valines, isoleucines and leucines. *Biochemistry* **40**, 13998–14003 (2001).
29. G. Saelensminde, Ø. Halskau Jr., R. Helland, N. P. Willassen, I. Jonassen, Structure-dependent relationships between growth temperature of prokaryotes and the amino acid frequency in their proteins. *Extremophiles* **11**, 585–596 (2007).
30. S. Moon, J. Kim, J. Koo, E. Bae, Structural and mutational analyses of psychrophilic and mesophilic adenylate kinases highlight the role of hydrophobic interactions in protein thermal stability. *Struct. Dyn.* **6**, 024702 (2019).
31. V. Makarov, B. M. Pettitt, M. Feig, Solvation and hydration of proteins and nucleic acids: A theoretical view of simulation and experiment. *Acc. Chem. Res.* **35**, 376–384 (2002).
32. N. Macro *et al.*, Slowdown of water dynamics from the top to the bottom of the GroEL cavity. *J. Phys. Chem. Lett.* **12**, 5723–5730 (2021).
33. D. Lucent, V. Vishal, V. S. Pande, Protein folding under confinement: A role for solvent. *Proc. Natl. Acad. Sci. U.S.A.* **104**, 10430–10434 (2007).
34. E. J. Sorin, V. S. Pande, Nanotube confinement denatures protein helices. *J. Am. Chem. Soc.* **128**, 6316–6317 (2006).
35. B. Bandyopadhyay *et al.*, Local energetic frustration affects the dependence of green fluorescent protein folding on the chaperonin GroEL. *J. Biol. Chem.* **292**, 20583–20591 (2017).